


ORIGINAL ARTICLE

Anti-signal recognition particle antibodies induce cardiac diastolic dysfunction via oxidative stress injury

Hao Zhang^{1,2,3,a} , Yunjing Shi^{4,5,a}, Yingze Fan^{4,5}, Dehao Zhu¹, Zeping Qiu^{4,5}, Huihui Chi¹, Qiongyi Hu¹, Liangzhe Xie⁶, Yue Sun¹, Honglei Liu¹, Xiaobing Cheng¹, Junna Ye¹, Hui Shi¹, Zhuochao Zhou¹, Jianfen Meng¹, Jialin Teng¹, Chengde Yang¹, Wei Jin⁵ & Yutong Su^{1,7}

¹Department of Rheumatology and Immunology, Ruijin Hospital, Shanghai Jiao Tong University School of Medicine, Shanghai, China

²Department of Rheumatology and Immunology, The First Hospital of Lanzhou University, Lanzhou, Gansu, China

³The First Clinical Medical College, Lanzhou University, Lanzhou, Gansu, China

⁴Department of Cardiovascular Medicine, Ruijin Hospital, Shanghai Jiao Tong University School of Medicine, Shanghai, China

⁵Department of Cardiovascular Medicine, Heart Failure Center, Ruijin Hospital, and Ruijin Hospital Lu Wan Branch, Shanghai Jiao Tong University School of Medicine, Shanghai, China

⁶Department of Laboratory Medicine, Ruijin Hospital, Shanghai Jiao Tong University School of Medicine, Shanghai, China

⁷Shanghai Hospital of Civil Aviation Administration of China, Shanghai, China

Correspondence

Y Su, Department of Rheumatology and Immunology, Ruijin Hospital, Shanghai Jiao Tong University School of Medicine, No. 197 Ruijin Second Road, Shanghai 200025, China.
E-mail: suyt2015@163.com

W Jin, Department of Cardiovascular Medicine, Heart Failure Center, Ruijin Hospital, and Ruijin Hospital Lu Wan Branch, Shanghai Jiao Tong University School of Medicine, Shanghai 200025, China.
E-mail: jinwei@shsmu.edu.cn

^aEqual contributors.

Received 14 January 2024;

Revised 24 May and 26 July 2024;

Accepted 28 July 2024

doi: 10.1002/cti.1525

Clinical & Translational Immunology
2024; 13: e1525

Abstract

Objectives. Anti-signal recognition particle (SRP) antibodies, markers of immune-mediated necrotising myopathy, are reportedly related to cardiac involvement; however, whether they are pathogenic to the myocardium remains unclear. We aimed, therefore, to explore the pathogenicity of anti-SRP antibodies against the myocardium through *in vivo* and *in vitro* studies.

Methods. Total immunoglobulin G (IgG), purified from patients with positive anti-SRP antibodies, was passively transferred into C57BL/6 mice. Cardiac function was evaluated via echocardiography and the ventricular pressure–volume loop; cardiac histological changes were analysed using haematoxylin–eosin staining, picrosirius red staining, immunofluorescence and immunohistochemistry. Additionally, reactive oxygen species (ROS) formation was evaluated by dihydroethidium (DHE) staining; mitochondrial morphology and function were evaluated using transmission electron microscopy and Seahorse mitochondrial respiration assay, respectively. The myositis cohort at our centre was subsequently reviewed in terms of cardiac assessments.

Results. After the passive transfer of total IgG from patients with positive anti-SRP antibodies, C57BL/6 mice developed significant left ventricular diastolic dysfunction (LVDD). Transcriptomic analysis and corresponding experiments revealed increased oxidative stress and mitochondrial damage in the hearts of the experimental mice. Cardiomyocytes exposed to anti-SRP-specific IgG, however, recovered normal mitochondrial metabolism after treatment with N-acetylcysteine, an ROS scavenger. Moreover, patients positive for anti-SRP antibodies manifested worse diastolic but equivalent systolic function compared to their counterparts after propensity score matching. **Conclusion.** Anti-SRP antibodies

may play a pathogenic role in the development of LVDD by promoting ROS production and subsequent myocardial mitochondrial impairment. The inhibition of oxidative stress was effective in reversing anti-SRP antibody-induced LVDD.

Keywords: anti-signal recognition particle antibody, left ventricular diastolic dysfunction, mitochondrial injury, myositis, reactive oxygen species

INTRODUCTION

Anti-signal recognition particle (SRP) antibodies, first identified by Reeves¹ in 1986, are markers of immune-mediated necrotising myopathy (IMNM). Anti-SRP-positive myopathy, a subgroup of idiopathic inflammatory myopathy (IIM), often referred to as myositis, is related to severe skeletal muscle weakness and increased creatine kinase (CK) levels.^{2,3} Myocardial involvement is a frequent complication of myositis and is usually associated with a poor prognosis.^{4,5} Previous evidence suggested a link between anti-SRP antibodies and high rates of cardiac involvement; however, the full relationship remains to be elucidated.^{6,7} Cardiac involvement in patients positive for anti-SRP antibodies is heterogeneous, ranging from subclinical damage to life-threatening arrhythmia or heart failure.⁸ We recently reported an inclination to develop heart failure with preserved ejection fraction in anti-SRP⁺ myositis patients.⁹

The anti-signal recognition particle is a ribonucleoprotein complex composed of six polypeptide chains, among which the 54 kDa polypeptide (SRP54) is the main functional subunit. SRP is primarily localised in the endoplasmic reticulum, where it recognises and translocates polypeptide chains.¹⁰ Additionally, several studies have reported the pathogenicity of anti-SRP antibodies in IIM. A longitudinal clinical study revealed a positive correlation of anti-SRP antibody titres to CK levels and disease activity scores.¹¹ A favorable response to B-cell depletion therapy with rituximab and plasma exchange also suggested an immune-mediated pathogenic mechanism underlying anti-SRP-positive myopathy.^{12,13} Furthermore, serum containing anti-SRP antibodies was shown to reduce the viability of myoblasts and mediate necrosis of skeletal muscles in mice.^{14,15} Herein, anti-SRP antibodies serve not only as disease

biomarkers, but also exert direct pathogenic effects against skeletal muscles.¹⁶

Since the expression of SRP is ubiquitous rather than muscle specific and the myocardium shares analogous features with skeletal muscles, it can be assumed that they are likely to be affected by the same pathogenic process. Muscle histology in anti-SRP-positive myopathy often demonstrates massive necrotic fibres with minimal inflammation,^{17,18} and a recent myocardial biopsy study revealed similar pathological lesions in the cardiac muscles of an anti-SRP-positive patient.¹⁹ The pathogenicity of anti-SRP antibodies towards the myocardium, however, has not yet been experimentally verified. In the present study, therefore, we performed *in vivo* and *in vitro* experiments to explore whether anti-SRP antibodies affect the myocardium and briefly investigated the underlying mechanism.

RESULTS

Reactivity of human autoantibodies against their cognate murine targets

First, we purified total IgG and anti-SRP-specific IgG from the patient plasma and confirmed it using Coomassie brilliant blue staining (Supplementary figure 1). The binding of immunoaffinity-purified anti-SRP-specific IgG to the recombinant human SRP54 protein was verified by western blotting (Figure 1a). The cross-reaction between immunoaffinity-purified anti-SRP-specific IgG and the SRP antigen was demonstrated by enzyme-linked immunosorbent assay (Supplementary table 1), as well as a commercial test line (Supplementary figure 2). Since SRP54 is 100% conserved between humans and mice according to published studies,¹⁵ we then explored whether human source anti-SRP IgG would react with its cognate antigen in mice hearts. First of all,

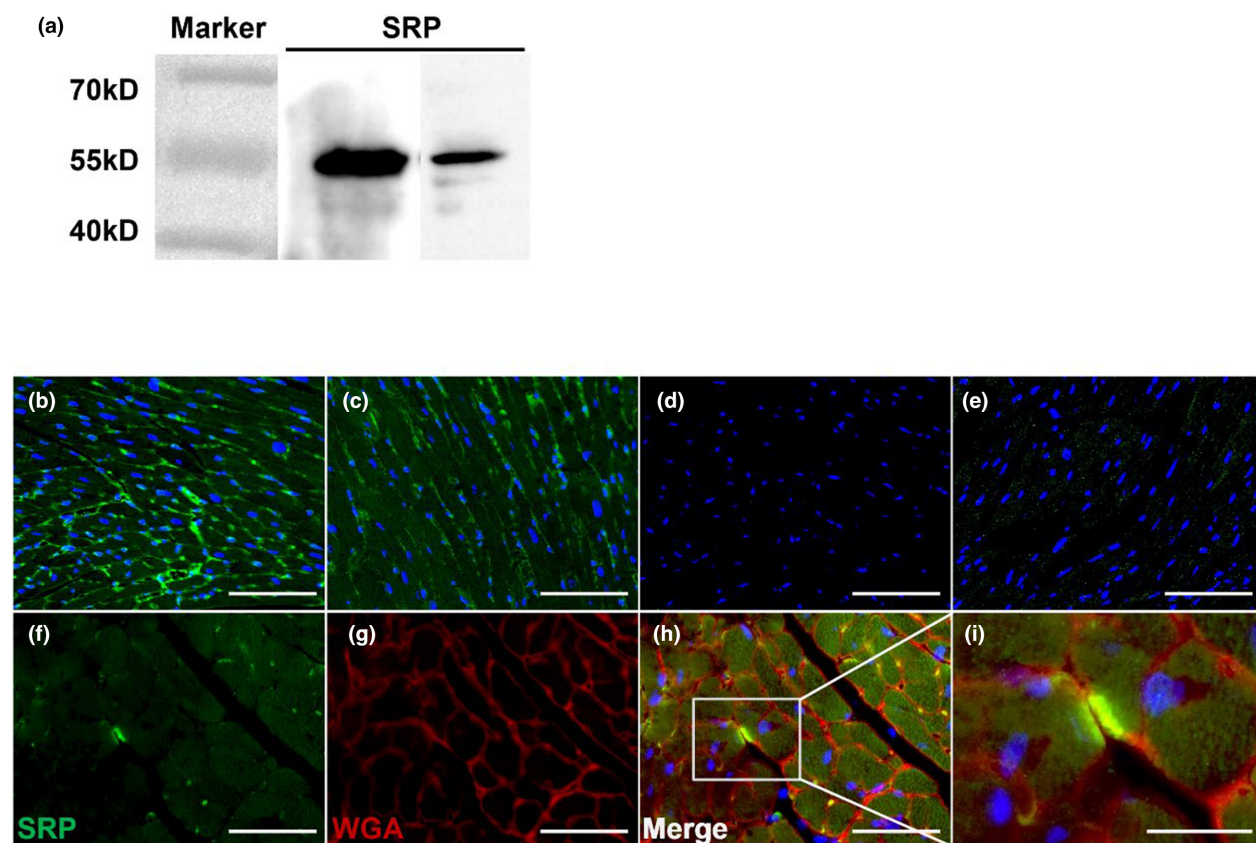


Figure 1. Immunoreactivity study of human source anti-SRP antibodies. **(a)** Western blot of recombinant SRP54 protein revealed by mouse anti-SRP antibody (line on the left) or immunoaffinity-purified human anti-SRP-specific IgG (line on the right). **(b–i)** Representative immunofluorescence staining of mouse myocardium after incubation with **(b)** mouse anti-SRP antibody and FITC-labelled anti-mouse secondary antibody, **(c)** immunoaffinity-purified anti-SRP-specific IgG from patient plasma and FITC-labelled anti-human secondary antibody, **(d)** purified total IgG from HCs' plasma and FITC-labelled anti-human secondary antibody, **(e)** immunoaffinity-purified anti-SRP-specific IgG from patient plasma with prior inhibition by free SRP54 protein and FITC-labelled anti-human secondary antibody and **(f–i)** immunoaffinity-purified anti-SRP-specific IgG from patient plasma (green) and co-staining with WGA (red) (Scale bar, 50 μm ; 20 μm for inset). All are counterstained with DAPI (blue). These experiments were repeated three times. SRP, signal recognition particle; WGA, wheat germ agglutinin.

the positive signal demonstrated the presence of immunoreactive SRP antigen in mice hearts when immunostained with commercial anti-SRP antibodies (Figure 1b). Moreover, anti-SRP-specific IgG from patients, but not healthy controls (HCs), recognised their targets in the mouse myocardium (Figure 1c and d). However, the signal disappeared in a competition experiment in which IgG was pre-incubated with recombinant SRP54 (Figure 1e). The co-localisation of immunoaffinity-purified anti-SRP-specific IgG from patients and wheat germ agglutinin (WGA) suggested a sarcolemmal expression pattern (Figure 1f–i). Taken together, these results showed that patient-derived anti-SRP IgG recognised its cognate antigenic targets in mice hearts.

***In vivo* pathogenicity of human source anti-SRP antibodies**

Based on the previous studies, we used a passive transfer method to investigate the pathogenicity of human source anti-SRP antibodies in mice. In brief, C57BL/6 mice received daily intraperitoneal injections of purified total IgG from anti-SRP⁺ myositis patients (anti-SRP⁺ group) or from the HC group, for 14 consecutive days. To limit xenotransplantation against human protein, the animals were transiently immunosuppressed with a single dose of cyclophosphamide (Figure 2a). After 14 days, the anti-SRP⁺ group exhibited a higher drop rate in the wire-hanging test after adjusting for body weight (Figure 2b and c), significant myofibre

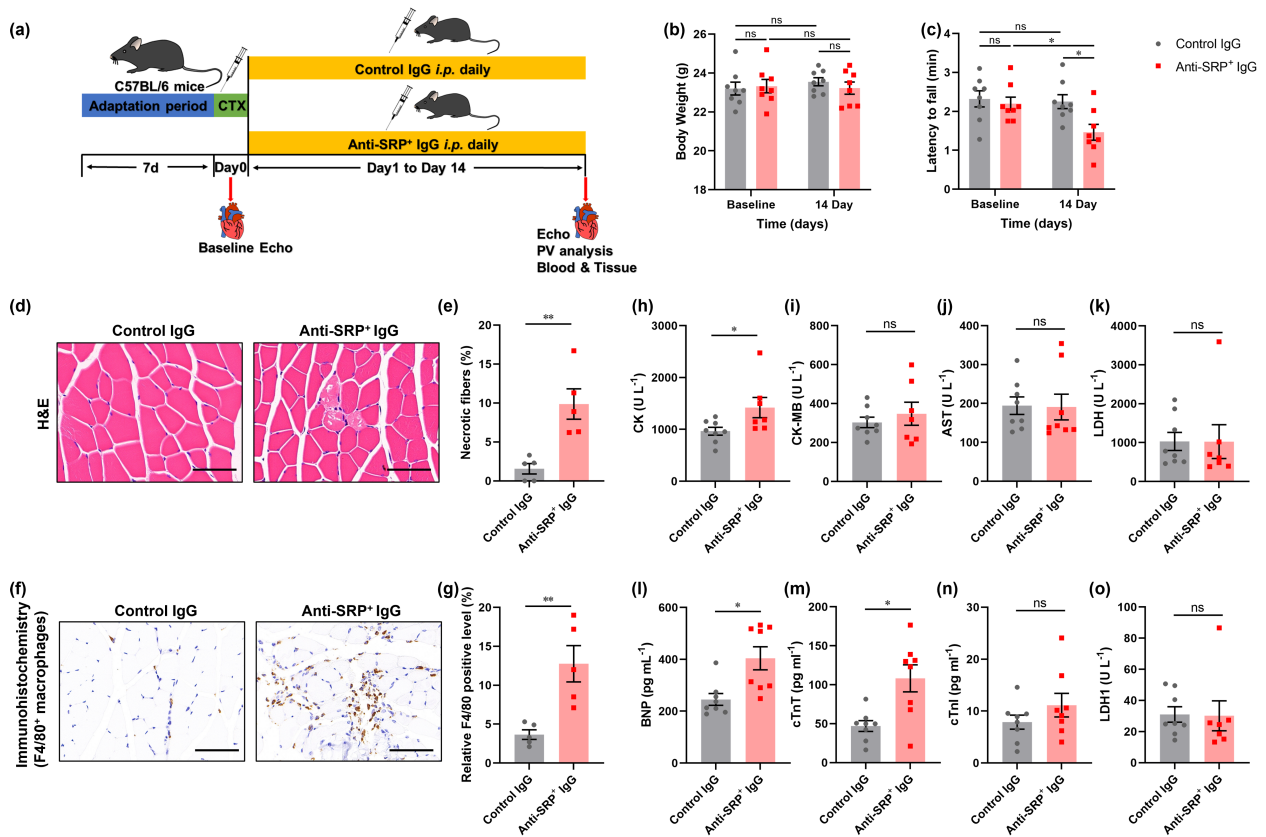


Figure 2. *In vivo* study of the pathogenicity of human source anti-SRP antibodies. **(a)** Experimental overview. **(b, c)** Body weight **(b)** and wire hanging time **(c)** of mice before and after injection of total IgG ($n = 8$). **(d)** H&E staining of muscle cryosection in each group (Scale bar, 50 μm). **(e)** Quantification of necrotic muscle fibres in triceps muscles in each group ($n = 5$ per group from 5 random fields per mice). **(f)** Immunohistological staining of F4/80⁺ macrophages in mice muscle fibres in each group (Scale bar, 50 μm). **(g)** The relative value of F4/80 positive levels in each group ($n = 5$ per group from 5 random fields per mouse). **(h–k)** The comparison of serum levels of CK **(h)**, CK-MB **(i)**, AST **(j)** and LDH **(k)** between two mice groups. **(l–o)** The comparison of serum levels of BNP **(l)**, cTnT **(m)**, cTnI **(n)** and LDH1 **(o)** between two mice groups ($n = 8$). All data are presented as mean \pm SEM. The data shown are from one of three experiments, which all showed similar results. ns $P > 0.05$, * $P < 0.05$, ** $P < 0.01$. AST, aspartate aminotransferase; BNP, B-type natriuretic peptide; CK, creatine kinase; CK-MB, creatine kinase-MB; cTnI, cardiac troponin I; cTnT, cardiac troponin T; CTX, cyclophosphamide; H&E, haematoxylin–eosin staining; HC, health control; IgG, immunoglobulin G; LDH, lactate dehydrogenase; SRP, signal recognition particle; LDH1, lactate dehydrogenase 1.

necrosis (Figure 2d and e) and macrophage infiltration (Figure 2f and g) in the muscle biopsy and higher serum CK levels (Figure 2h–k).

Human source anti-SRP antibodies caused cardiac diastolic dysfunction in mice

Subsequently, we explored the cardiac manifestations of mice injected with purified total IgG from anti-SRP⁺ myositis patients. Of note, cardiac biomarkers, including brain natriuretic peptide (BNP) and cardiac troponin T (cTnT), were markedly elevated (Figure 2l–o) in the experimental mice. Indicators reflecting systolic

function, such as left ventricular ejection fraction (LVEF) and cardiac ventricular dimensions, remained unchanged on M-mode echocardiography (Figure 3a–c, Supplementary figure 3). The anti-SRP⁺ group, however, tended to suffer from LVDD, characterised by decreased transmitral E/A and increased deceleration time on evaluation with pulsed-wave colour Doppler echocardiography (Figure 3d–f). Simultaneously, the mitral E velocity to mitral annular E' velocity ratio (E/E') on tissue Doppler imaging, which is a reliable predictor of left ventricular (LV) end-diastolic pressure, was also dramatically elevated in the experimental mice (Figure 3g–i).

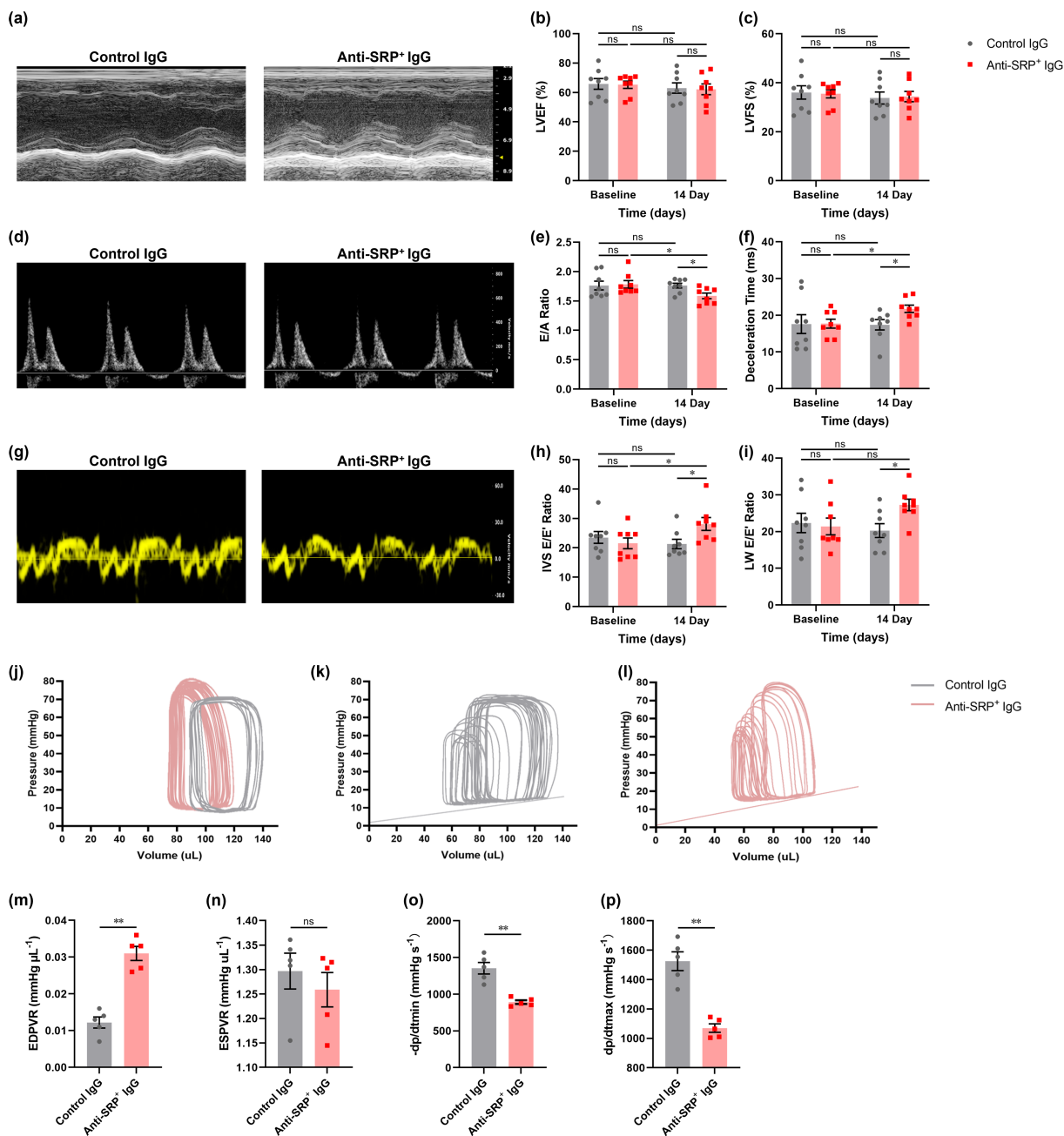


Figure 3. The decline in cardiac diastolic function in mice after injection of human source anti-SRP antibodies. **(a)** Representative images of left ventricular M-mode echocardiographic tracings of mice after injection with HC or anti-SRP IgG. **(b, c)** Percentages of LVEF **(b)** and LVFS **(c)** in two mice groups ($n = 8$). **(d)** Representative mitral flow patterns from pulsed-wave colour Doppler echocardiography in two mice groups. **(e, f)** The levels of E/A ratio **(e)** and deceleration time **(f)** in two mice groups ($n = 8$). **(g)** Representative images of mitral annular Doppler tissue imaging in two mice groups. **(h, i)** The levels of IVS E/E' ratio **(h)** and LW E/E' ratio **(i)** in two mice groups ($n = 8$). **(j–l)** Representative steady-state left ventricular pressure–volume (P–V) loops in two mice groups. **(m–p)** The diastolic stiffness coefficient β of EDPVR **(m)**, the ESPVR **(n)**, systolic contractility **(o)** and diastolic relaxation **(p)** were calculated from the P–V loop analysis in two mice groups ($n = 5$). All data are presented as mean \pm SEM. The data shown are from one of three experiments, which all showed similar results. ns $P > 0.05$, * $P < 0.05$, ** $P < 0.01$. HC, health control; IgG, immunoglobulin G; SRP, signal recognition particle; LVEF, left ventricular ejection fraction; LVFS, left ventricular fractional shortening; E/A, early diastolic filling velocity/atrial filling velocity ratio; IVS E/E', peak early diastolic velocity/peak early diastolic mitral annular velocity ratio at the septum of the left ventricle; LW E/E', peak early diastolic velocity/peak early diastolic mitral annular velocity ratio at the lateral wall of the left ventricle; EDPVR, end-diastolic pressure–volume relationship; ESPVR, end-systolic pressure–volume relationship.

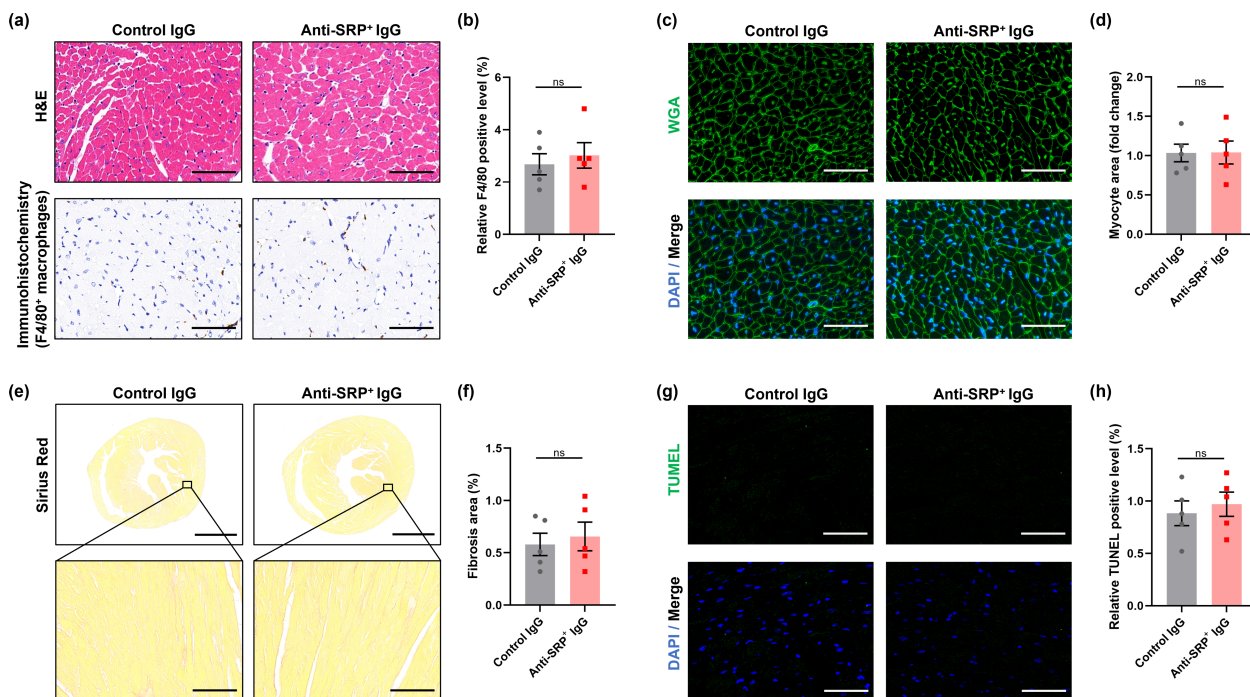


Figure 4. Cardiac serological and histological changes in mice after injection of human source anti-SRP antibodies. **(a)** H&E staining (upper) and immunohistological staining for F4/80⁺ macrophages (lower) of myocardium in each group (Scale bar, 50 μ m). **(b)** The relative value of F4/80 positive levels in each group ($n = 5$ per group from 5 random fields per mouse). **(c)** Representative immunofluorescent image of WGA staining of mice hearts in each group (Scale bar, 50 μ m; green, WGA; blue, DAPI). **(d)** The relative value of myocardial cell size of mice in each group ($n = 5$ per group from 5 random fields per mouse). **(e)** Sirius red staining of myocardium in each group (Scale bar, 1 mm; 50 μ m for inset). **(f)** Percentage of cardiac fibrosis area in each group ($n = 5$ per group from 5 random fields per mouse). **(g)** Representative immunofluorescent image of TUNEL staining of mice hearts in each group (Scale bar, 50 μ m; green, TUNEL; blue, DAPI). **(h)** The relative value of TUNEL positive levels in each group ($n = 5$ per group from 5 random fields per mouse). All data are presented as mean \pm SEM. The data shown are from one of three experiments, which all showed similar results. ns $P > 0.05$. H&E, haematoxylin–eosin staining; HC, health control; IgG, immunoglobulin G; SRP, signal recognition particle; TUNEL, terminal deoxynucleotidyl transferase dUTP nick-end labelling; WGA, wheat germ agglutinin.

To further assess real-time cardiac haemodynamics, pressure–volume analysis was performed via LV catheterisation (Figure 3j–l). The anti-SRP⁺ group showed significantly increased load-independent diastolic stiffness coefficient of the end-diastolic pressure–volume relationship (EDPVR) (Figure 3m), along with decreased load-dependent minimum and maximum LV pressure change ratios (dP/dt min, –dP/dt max; Figure 3o and p), suggesting LV chamber stiffness and relaxation impairment, respectively. In contrast, the end-systolic pressure–volume relationship (ESPVR), which reflects myocardial contractility, showed no difference between the two groups (Figure 3n). Collectively, the presence of diastolic dysfunction concomitant with LVEF preservation was validated via both non-invasive and invasive manners.

Human source anti-SRP antibodies exerted no effect on myocardial morphology, inflammatory infiltration, apoptosis or fibrosis

We then investigated pathophysiological changes in the myocardium of the anti-SRP⁺ group. No obvious disorganisation or necrosis was observed upon haematoxylin–eosin staining and no significant macrophage infiltration was observed by F4/80 staining (Figure 4a and b). In parallel, WGA staining showed similar cardiomyocyte sizes between the two groups (Figure 4c and d). Picrosirius red staining of the LV sections revealed a landscape of collagen deposition-free in the myocardium as well (Figure 4e and f). Further, no significant differences were observed in terms of cell apoptosis, as revealed by the terminal

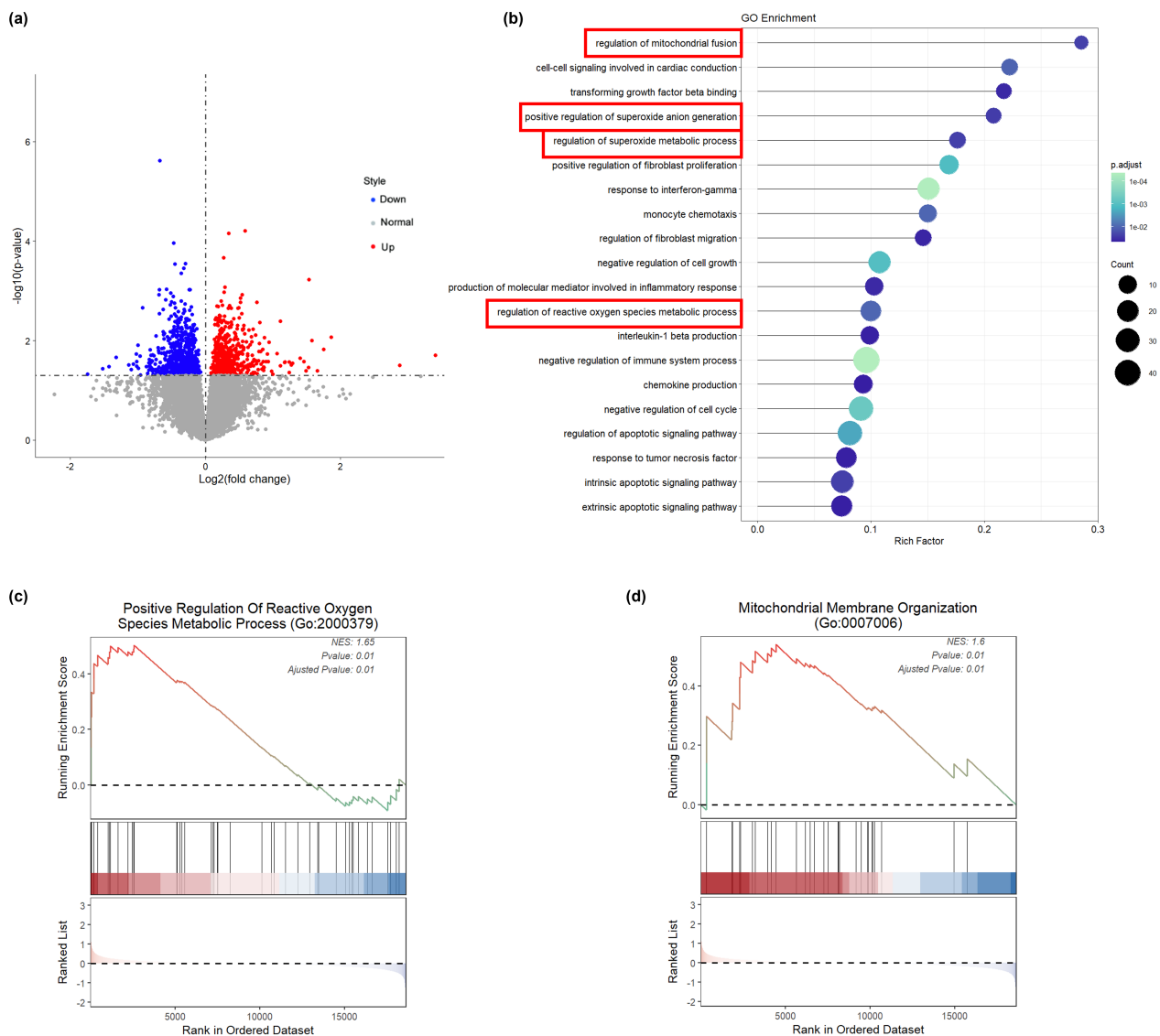


Figure 5. The upregulation of reactive oxygen species metabolic pathways in the transcriptomic analysis of mouse hearts. **(a)** Volcano plot showing significantly decreased (blue) and increased (red) genes. **(b)** Gene ontology (GO) analysis of RNA-sequencing data. **(c, d)** Gene set enrichment analysis of 'Positive Regulation of Reactive Oxygen Species Metabolic Process' **(c)** and 'Mitochondrial Membrane Organization' **(d)** pathways with all detected mRNAs ($n = 3$ per group).

deoxynucleotidyl transferase 2'-Deoxyuridine, 5'-Triphosphate (dUTP) nick-end labelling (TUNEL) assay (Figure 4g and h).

Human source anti-SRP antibodies influenced ROS production and mitochondrial function in mice hearts

To further explain the mechanism underlying the cardiac phenotype caused by anti-SRP antibodies, we performed a transcriptomic analysis of mice

hearts. A total of 1172 differentially expressed genes were identified, 655 of which were downregulated, while 517 were upregulated in the anti-SRP⁺ group. A volcano plot of differentially expressed genes is shown in Figure 5a. Gene ontology (GO) analysis revealed that multiple genes were involved in mitochondrial regulation, superoxide anion generation and ROS pathways (Figure 5b). Gene set enrichment analysis of all of the detected messenger ribonucleic acid (mRNA) further verified that ROS production and

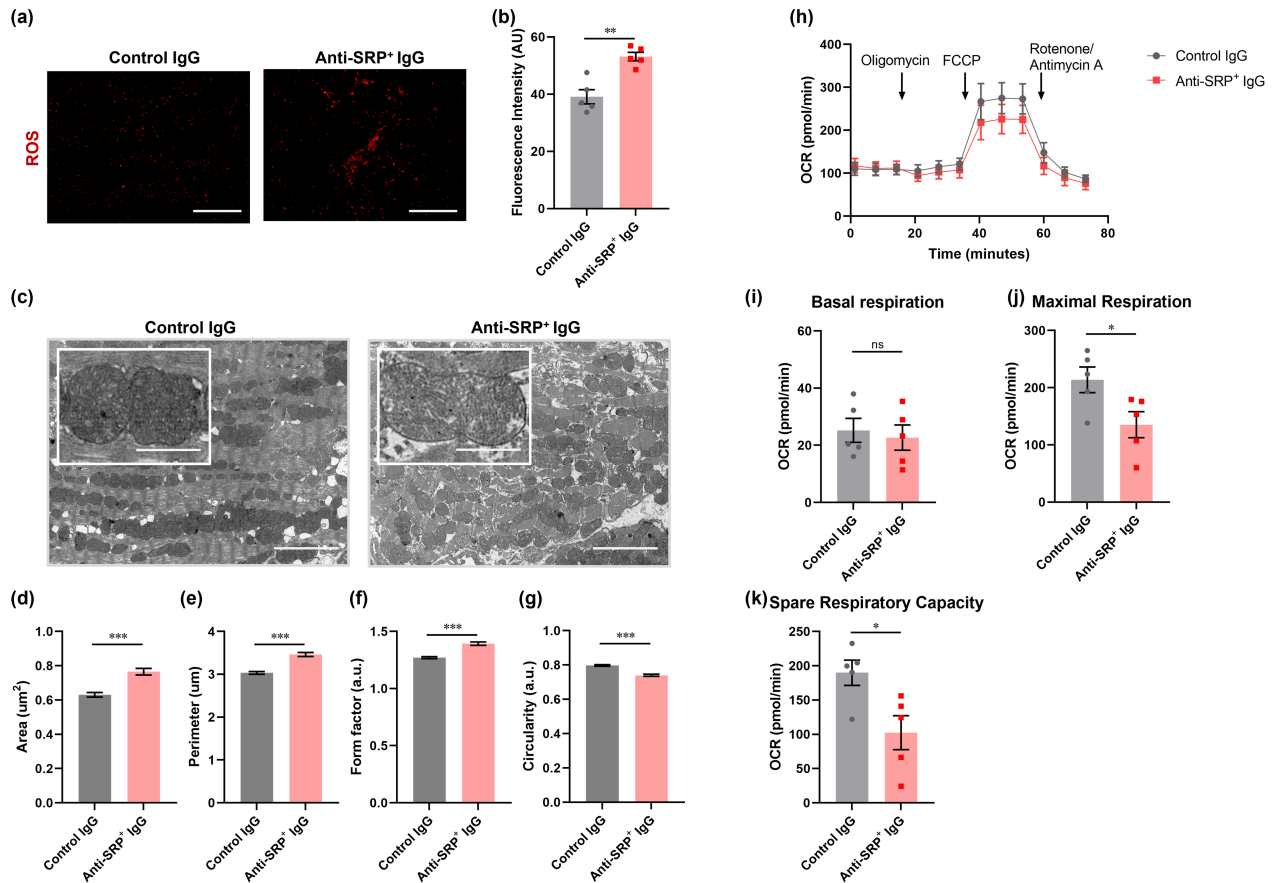


Figure 6. The alteration of mitochondrial integrity and function induced by increased ROS levels in mouse hearts. **(a, b)** Representative image **(a)** and summary fluorescence intensity **(b)** of DHE staining of myocardium for ROS formation ($n = 5$ per group from 5 random fields per mice; Scale bar, 50 μm). **(c)** Representative transmission electron microscopy images of cardiac tissue in each group (Scale bar, 5 μm; 1 μm for inset). **(d–g)** Quantification analysis of mitochondrial area **(d)**, mitochondrial perimeter **(e)**, mitochondrial form factor **(f)** and mitochondrial circularity **(g)** in each group (330 mitochondria per group). **(h)** Real-time mitochondrial respiration capacity monitoring the oxygen consumption rate in primary cardiomyocytes isolated in each group. **(i–k)** The basal respiration **(i)**, maximal respiration **(j)** and spare respiratory capacity **(k)** of primary cardiomyocytes isolated in each group ($n = 5$). All data are presented as mean ± SEM. The data shown are from one of three experiments, which all showed similar results. ns $P > 0.05$, * $P < 0.05$, ** $P < 0.01$, *** $P < 0.001$. ROS, reactive oxygen species; IgG, immunoglobulin G; SRP, signal recognition particle; FCCP, carbonyl cyanide-4 (trifluoromethoxy) phenylhydrazone; OCR, oxygen consumption rate; DHE, dihydroethidium.

mitochondrial injury were significantly enriched in the anti-SRP⁺ group (Figure 5c and d).

Human source anti-SRP antibodies increased cardiac ROS levels and altered mitochondrial integrity and function in mice

We next utilised DHE staining to evaluate the ROS levels and mitochondrial changes and observed increased ROS levels in the myocardium of the anti-SRP⁺ group (Figure 6a and b). Additionally, transmission electron microscopy showed altered

mitochondrial morphology, including swollen outer membranes (Figure 6c), increased mitochondrial perimeters (Figure 6d and e) and increased form factors, along with decreased circularity (Figure 6f and g).

To evaluate the functional consequences of the disturbance in the ultrastructural integrity of the mitochondrial architecture, we evaluated the bioenergetic function of isolated primary cardiomyocytes from each group, via oxygen consumption rate measurements obtained using a Seahorse XF Analyser (Figure 6h). Extracellular flux analysis showed that spare and maximal

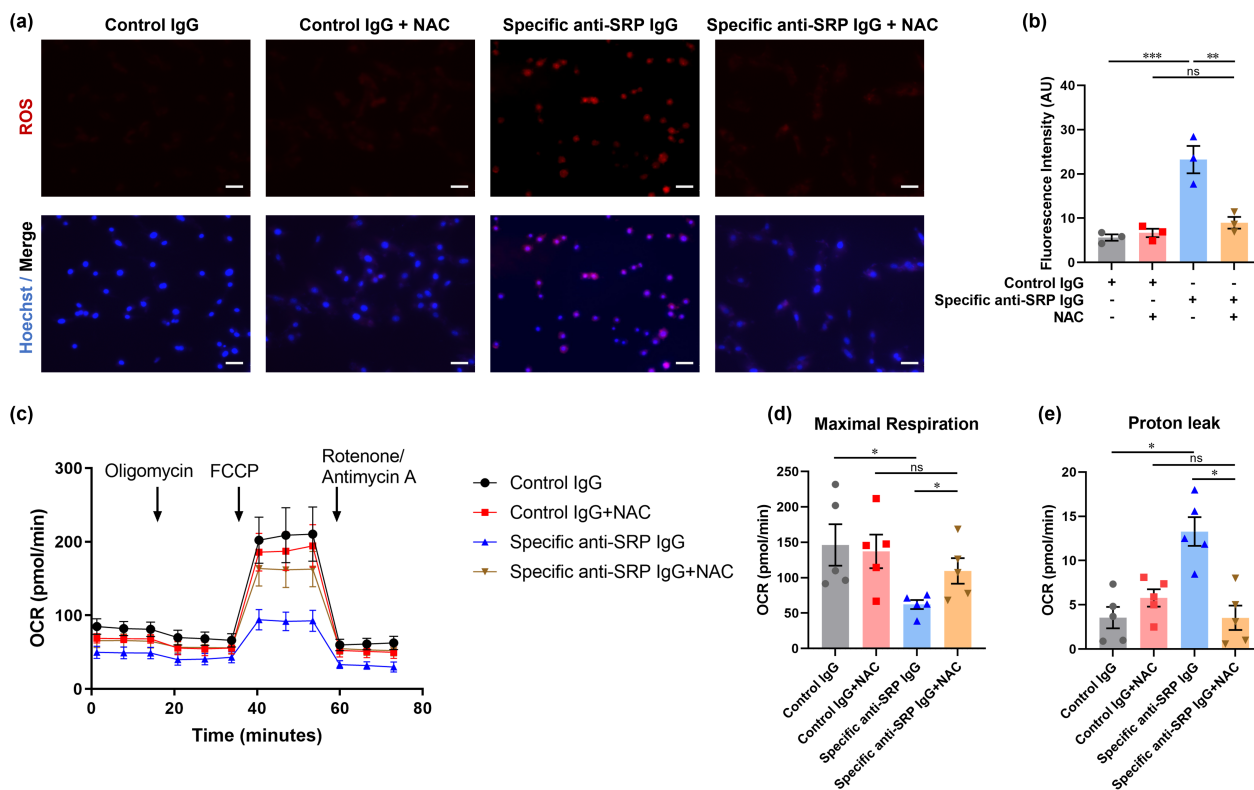


Figure 7. NAC reversed the oxidative stress effect of immunoaffinity-purified-specific anti-SRP antibodies on neonatal rat ventricular myocytes. **(a, b)** Representative image **(a)** and summary fluorescence intensity **(b)** of DHE staining of neonatal rat ventricular myocytes cultured with immunoaffinity-purified-specific anti-SRP IgG or purified IgG from HCs, treated with or without NAC ($n = 3$ per group from 3 random fields; Scale bar, 50 μm). **(c)** Real-time mitochondrial respiration capacity monitoring the oxygen consumption rate in neonatal rat ventricular myocytes in each group. **(d, e)** The maximal respiration **(d)** and proton leak **(e)** in neonatal rat ventricular myocytes in each group ($n = 5$). All data are presented as mean \pm SEM. The data shown are from one of three experiments, which all showed similar results. ns $P > 0.05$, * $P < 0.05$, ** $P < 0.01$, *** $P < 0.001$. DHE, dihydroethidium; FCCP, carbonyl cyanide-4 (trifluoromethoxy) phenylhydrazone; IgG, immunoglobulin G; NAC, N-acetylcysteine; OCR, oxygen consumption rate; SRP, signal recognition particle.

respiration capacities were markedly reduced in the anti-SRP⁺ group (Figure 6i–k), while the basal respiration capacity was unaffected.

N-acetylcysteine treatment reversed mitochondrial dysfunction in cardiomyocytes exposed to immunoaffinity-purified anti-SRP-specific IgG

To further elucidate the direct pathogenic effects of anti-SRP antibodies on cardiomyocytes, we added immunoaffinity-purified anti-SRP-specific IgG from patients to the cultures of cardiomyocytes *in vitro*. Considering that the cell line did not completely exhibit the properties of cardiomyocytes, the experiments were performed using neonatal rat ventricular myocytes (NRVMs).

A-actinin was used as a positive marker to identify NRVMs (Supplementary figure 4). It turned out that immunoaffinity-purified anti-SRP-specific IgG induced higher ROS levels in NRVMs, which was reversed by the antioxidant N-acetylcysteine (NAC) (Figure 7a and b). Furthermore, NAC supplementation attenuated the damage to mitochondrial oxidative phosphorylation in NRVMs, as revealed by real-time mitochondrial respiration detection (Figure 7c–e).

Increased tendency to develop cardiac diastolic dysfunction in patients with anti-SRP antibodies

Based on the aforementioned findings, we then explored the clinical relevance of our myositis cohort ($n = 253$) with anti-SRP antibodies ($n = 41$).

Table 1. Selected patient characteristics in myositis patients stratified by anti-SRP positivity versus anti-SRP negativity after propensity score weighting

	Anti-SRP positivity (n = 38)	Anti-SRP negativity (n = 76)	P-value
Age (year, median, IQR)	56.5 (49.8–64.3)	58.5 (48.3–65.0)	0.935
Sex (female/male)	27/11	52/24	0.774
Duration (month, median, IQR)	4.0 (1.8–12.0)	4.0 (2.0–12.0)	0.966
BMI (kg/m ² , median, IQR)	22.6 (20.7–25.2)	22.9 (20.2–25.2)	0.921
Cardiovascular risk factors (n, %)			
Hypertension	6 (15.8)	11 (14.5)	0.853
Diabetes mellitus	6 (15.8)	12 (15.8)	0.999
Hyperlipaemia	2 (5.3)	5 (6.6)	0.783
Smoking history	1 (2.6)	1 (1.3)	0.614
Laboratory values (median, IQR)			
CK (IU L ⁻¹)	245.5.0 (62.0–3440.0)	93.5 (58.0–386.5)	0.037
CK-MB (ng mL ⁻¹)	11.9 (1.3–137.5)	2.7 (1.2–13.0)	0.021
cTnl (ng mL ⁻¹)	0.02 (0.01–0.06)	0.01 (0.01–0.03)	0.036
Mb (ng mL ⁻¹)	92.0 (16.2–871.2)	34.9 (16.8–84.1)	0.044
LDH (IU L ⁻¹)	392.0 (248.0–849.0)	287.5 (220.0–414.5)	0.011
NT-proBNP (pg mL ⁻¹)	142.5 (50.1–252.7)	98.3 (44.0–165.9)	0.040
Echocardiography (median, IQR)			
LAD (mm)	28.0 (24.0–32.0)	27.0 (25.0–29.0)	0.837
LVEDD (mm)	46.0 (42.0–50.0)	46.0 (44.0–48.8)	0.715
LVESD (mm)	25.0 (22.0–27.0)	26.5 (22.0–28.0)	0.106
IVST (mm)	9.0 (8.0–10.0)	9.0 (8.0–9.0)	0.201
LVPWT (mm)	9.0 (8.0–9.0)	8.0 (8.0–9.0)	0.015
LVEF (%)	68.0 (64.0–72.0)	69.0 (66.0–71.0)	0.468
E/A	0.9 (0.7–1.1)	1.0 (0.8–1.2)	0.020
Septal E' (m s ⁻¹)	7.7 (5.9–9.7)	8.3 (7.0–9.6)	0.245
Septal E/E'	10.4 (9.0–11.8)	9.0 (7.4–10.4)	0.028
Lateral E' (m s ⁻¹)	9.2 (6.9–11.7)	10.9 (9.0–11.8)	0.040
Lateral E/E'	8.2 (6.8–9.6)	7.4 (5.5–8.9)	0.049

Values are presented as median with interquartile range for continuous variables and as numbers with percentages for categorical variables. $P < 0.05$ is shown in bold type.

BMI, body mass index; CK, creatine kinase; CK-MB, creatine kinase-MB; cTnl, cardiac troponin I; E/A, early diastolic filling velocity/atrial filling velocity ratio; IQR, interquartile range; IVST, interventricular septal wall thickness; LAD, left atrial diameter; Lateral E', peak early diastolic mitral annular velocity at the lateral wall of the left ventricle; Lateral E/E', peak early diastolic velocity/peak early diastolic mitral annular velocity ratio at the lateral wall of the left ventricle; LDH, lactate dehydrogenase; LVEDD, left ventricular end-diastolic diameter; LVEF, left ventricular ejection fraction; LVESD, left ventricular end-systolic diameter; LVPWT, left ventricular posterior wall thickness; Mb, myoglobin; NT-proBNP, N-terminal pro-B-type natriuretic peptide; PSM, propensity score matching; Septal E', peak early diastolic mitral annular velocity at the septum of the left ventricle; Septal E/E', peak early diastolic velocity/peak early diastolic mitral annular velocity ratio at the septum of the left ventricle; SRP, signal recognition particle.

After propensity score matching (PSM), all pre- and intraoperative factors were well balanced between the anti-SRP⁺ group (n = 38) and its counterparts (n = 76) (Table 1).

When it came to cardiac assessments, we found that the anti-SRP⁺ group showed a more pronounced elevation of serological muscle enzymes and cardiac biomarkers levels. In particular, a considerable trend towards concentric hypertrophy and diastolic dysfunction, as indicated by echocardiographic parameters, was observed. Patients with anti-SRP antibodies displayed a decreased E/A ratio ($P = 0.020$) and lateral E' wave ($P = 0.040$) and an increased LV posterior wall

thickness ($P = 0.015$), septal E/E' ($P = 0.028$) and lateral E/E' ($P = 0.049$). Nonetheless, there were no significant differences between the two groups in terms of LVEF or LV volume (all $P > 0.05$). Above all, patients with anti-SRP antibodies tended to develop LVDD with contractile function preservation.

DISCUSSION

Previous research has revealed that anti-SRP antibodies act not only as serological markers for the IMNM subtype, but also as pathogenic factors directly involved in myoblast injury. Here, we showed, for the first time, that human source

anti-SRP antibodies induced diastolic dysfunction *in vivo*. In parallel, based on our clinical myositis cohort, we found that anti-SRP⁺ myositis patients were more susceptible to developing LVDD, characterised by myocardial relaxation impairment and centripetal hypertrophy, than their counterparts. Previous studies found that LVDD is an early feature of cardiac involvement in myositis patients; however, we first reported the SRP antibody-related LVDD phenotype basically and clinically. LVDD is closely associated with heart failure,^{20–22} so clinicians should be alert to early alterations in cardiac dysfunction in patients with anti-SRP antibodies.

Anti-SRP antibodies have been found to disturb the translocation of secretory proteins into the endoplasmic reticulum by binding to the SRP54 subunit and subsequently suppressing the SRP receptor-mediated release of endoplasmic reticulum signal sequences.²³ The mechanisms through which these circulatory autoantibodies reach their intracellular molecular targets, however, remain unclear. Presumably, intracellular antigens can be expressed ectopically at the cell surface under specific conditions or autoantibodies may enter the cells. For example, the endoplasmic reticulum protein calnexin is expressed on the surface of various cells, such as murine splenocytes, fibroblast cells and human HeLa cells.²⁴ Anti-deoxyribonucleic acid (DNA) antibodies enter living cells by binding to myosin on the cell membrane, thereby inhibiting the activity of nucleic acid endonucleases.^{25,26} Previous studies have shown that SRP antigen can be expressed on the surface of muscle fibrils.¹⁴ In line with these studies, we observed a similar sarcolemmal expression pattern of the SRP antigen in the myocardium, as revealed by the colocalisation of immunoaffinity-purified anti-SRP-specific IgG from patients and WGA by immunofluorescence staining. Nonetheless, whether anti-SRP antibodies enter the cardiomyocytes or cross-react with receptors on the cardiomyocyte surface requires further investigation.²⁷

To determine the cascade effects triggered by anti-SRP antibodies that contribute to the LVDD phenotype, we performed myocardial histological and transcriptomic analyses. With regular pathological changes, including hypertrophy, fibrosis, apoptosis, necrosis and inflammatory infiltration, being negative, ROS pathway activation was found to be the driving force behind this phenotype. Subsequent experiments further revealed the pathogenicity of oxidative stress by

damaging cardiac mitochondria, leading to oxygen utilisation disorders and energy deficits. Myocardial mitochondrial abnormality is a critical feature of LVDD. Several mouse models of cardiac hypertrophy and diastolic dysfunction have shown significant decreases in cardiac mitochondrial metabolism and a mismatch between adenosine triphosphate (ATP) production and demand.^{28,29} Throughout the cardiac cycle, diastole is the most energy-demanding phase; therefore, the vicious cycle between ROS and mitochondria aggravates the cardiac compliance decline and diastolic dysfunction.³⁰

Furthermore, Daniela *et al.*³¹ suggested that the attenuation of oxidative stress would help improve diastolic function by restoring myocardial energetics. Dan *et al.*³² reported that nicotinamide adenine dinucleotide (NAD⁺) precursor nicotinamide riboside supplementation was beneficial in diastolic function recovery in preclinical animal models. Several clinical trials of mitochondria-targeted therapies are ongoing and are recognised to hold great promise for LVDD treatment.²⁹ In the present study, the restoration of oxygen consumption and energy metabolism was observed in primary cardiomyocytes treated with NAC, a type of ROS salvage. Of note, ROS activation and mitochondrial dysfunction in the skeletal muscles have also been reported to play pivotal roles in IIM.³³ Danli *et al.*³⁴ proposed several small-molecule compounds that targeted the mitochondrial pathway in juvenile dermatomyositis. Our results support the pathogenicity of the mitochondrial redox imbalance in IIM mice with LVDD. Therefore, ROS inhibition is a promising strategy in the treatment of IIM patients with cardiac involvement. Its safety and effectiveness, however, need to be further verified in animal and clinical studies.

The present study had several limitations. First, we briefly demonstrated the pathogenicity of anti-SRP antibodies against the myocardium through the oxidative stress pathway; however, the mechanism by which these autoantibodies bind to their target in the heart remains to be fully elucidated. Moreover, because of the xenogenic response elicited against human IgG, we were hindered from observing the extended *in vivo* effects of anti-SRP antibodies on the myocardium. Finally, we observed a tendency for anti-SRP⁺ patients to develop LVDD by evaluating the baseline echocardiograms in our myositis cohort; however, a long-term follow-up study should be conducted to further confirm the association between anti-SRP antibodies and LVDD.

METHODS

Patients

A total of 253 IIM patients admitted to the Department of Rheumatology and Immunology, Ruijin Hospital from January 2016 to October 2022 were enrolled. All patients fulfilled the Bohan and Peter IIM criteria or 2004 European Neuromuscular Centre (ENMC) criteria.^{35,36} Patients with a history of coronary artery disease, severe lung infection or evidence of malignancy were excluded. To reduce selection bias and make the anti-SRP antibodies the only exposure, 1:2 nearest-neighbour PSM was created using the following baseline characteristics: age, sex, duration, body mass index, hypertension, diabetes mellitus, hyperlipaemia, obesity and smoking history.

Human samples and IgG purification

Plasmas were obtained from two patients with anti-SRP⁺ antibodies after the first plasma exchange. Plasma exchange was performed for therapeutic purposes. Total IgG was purified from plasma by a Protein G Agarose Prepacked Column (Beyotime, Shanghai, China) and concentrated in a centrifuge tube (Amicon) (Millipore, Darmstadt, Germany). The flow-through of IgG purification was kept for use as IgG-depleted control. Anti-SRP-specific IgG was purified by immunoaffinity chromatography on HiTrap NHS-Activated HP column (Cytiva, Washington, USA). In brief, recombinant human SRP54 protein (ProSpec-Tany, Ness-Ziona, Israel) was coupled to the column. Then, purified total IgG from patients with anti-SRP antibodies was used to pass through the column and followed by elution to obtain anti-SRP-specific IgG. Purified IgG without anti-SRP antibodies from healthy blood donors by the same procedure was used as control IgG. Furthermore, purified IgG was quantified by BCA assay (Beyotime, Shanghai, China) and confirmed by Coomassie Brilliant Blue staining (Beyotime, Shanghai, China). After sterile filtration, the samples were stored at -80°C until use.

Western blots

Western blots were performed using recombinant human SRP54 protein after 10% SDS-PAGE and transfer to a polyvinylidene difluoride membrane (Millipore, Darmstadt, Germany). The membrane was incubated with mouse anti-SRP antibody (Santa Cruz Biotechnology, Texas, USA) or immunoaffinity-purified anti-SRP-specific IgG from humans and incubated using secondary anti-mouse horseradish peroxidase (Cell Signal Technology, Boston, USA) or secondary anti-human horseradish peroxidase (Cell Signal Technology, Boston, USA), respectively. An electrochemiluminescence assay was used for the final visualisation.

Passive transfer of human IgG into mice

The 8–10-week-old female wild-type C57BL/6 mice were purchased from Charles River Laboratories (Beijing, China) and were divided into two groups of 8 animals. They received daily intraperitoneal injections of 2 mg of total IgG

purified from patients with anti-SRP antibodies or healthy donors for 14 days. To reduce anti-human xenogeneic immune responses, wild-type mice received a single dose of 300 mg kg^{-1} of cyclophosphamide (BaxterOncology, Halle, Germany) before the administration.

Wire hang test

The test began with the mice hanging from an elevated wire cage top. The animal was placed on the cage top, which was then inverted and suspended above the home cage; the latency to when the animal fell was recorded. This test was performed three times for each animal at intervals of more than 10 min.

Echocardiography

The echocardiography was performed in 1% isoflurane-anaesthetised C57BL/6 mice by Visual Sonics Vero 2100 system (Visual Sonics, Toronto, Canada). The animals' chests were shaved and hair removal gel was applied to minimise resistance to ultrasonic beam transmission. The parameters such as left ventricular ejection fraction (LVEF), left ventricular fractional shortening (LVFS), early diastolic filling velocity/atrial filling velocity ratio (E/A), deceleration time, peak early diastolic velocity/peak early diastolic mitral annular velocity ratio at the septum (IVS E/E') and lateral wall (LW E/E') of the left ventricle, interventricular septal wall thickness (IVST); systole, IVST; diastole, left ventricular posterior wall thickness (LVPWT); systole, LVPWT; diastole, left ventricular internal dimension (LVID); systole, LVID; diastole, stroke volume, cardiac output and left ventricular mass were all achieved and recorded.

Pressure–volume loop analysis

An *in vivo* pressure–volume analysis was performed in mice using a SciSense Advantage Admittance Derived Volume Measurement System and 1.2F catheters with 4.5 mm electrode spacing (Transonic Systems Inc., New York, USA). Mice were anaesthetised and ventilated with 1% isoflurane using an SAR-1000 Ventilator (CWE Inc, Ardmore, USA). Anaesthetised mice were secured and a bilateral subcostal incision was made. The diaphragm was opened to expose the heart. The catheter was inserted into the LV via an apical approach. The IVC was located and occluded during a sigh in ventilation to acquire load-independent indexes. Data acquisition and analysis were performed in LabScribe2 (iWorx, Dover NH, USA).

Histology, immunohistochemistry and immunofluorescence

Mice muscle and heart tissue were fixed with 4% paraformaldehyde, embedded in paraffin and dissected into 5- μm -thick sections. After de-waxing and rehydration, the sections were stained with haematoxylin and eosin (Beyotime, Shanghai, China), Sirius red (Leagene Biotechnology, Beijing, China), wheat germ agglutinin (Thermo Scientific, Massachusetts, USA) or antibodies against F4/80 (Abcam,

Cambridge, UK) for analysis. For immunofluorescence analysis of anti-SRP reactivity, cardiac tissue sections were incubated with monoclonal mouse anti-SRP antibody or immunoaffinity-purified anti-SRP-specific IgG from patients followed by FITC-labelled anti-mouse secondary antibody or FITC-labelled anti-human secondary antibody, respectively. DNA was stained with DAPI (Beyotime, Shanghai, China). Purified IgG from healthy control plasma was used for negative controls for staining specificity.

Terminal deoxynucleotidyl transferase-mediated dUTP nick end labelling

The ApopTag Peroxidase *In Situ* Apoptosis Detection Kit (Millipore, Darmstadt, Germany) was used according to the manufacturer's instructions for the detection of TUNEL-positive cells in cardiac tissue sections.

Detection of reactive oxygen species production

To detect the ROS generation in NRVMs, the 5×10^4 cells in a final volume of 500 μL were incubated for 20 min with 5 μM dihydroethidium (Beyotime, Shanghai, China) and then washed with serum-free DMEM three times. The nucleus was counterstained with Hoechst 33342 (Beyotime, Shanghai, China). The fluorescence images of intracellular ROS were acquired by using fluorescence microscopy (Olympus IX51, Tokyo Japan). The average fluorescence intensity was analysed by ImageJ.

RNA sequencing and analysis

Left ventricular tissues from mice were used for total RNA isolation. Oligo(dT)-attached magnetic bead purified mRNA was fragmented into pieces at the appropriate temperature. cDNA was generated by random hexamer-primed reverse transcription. Afterwards, RNA Index Adapters and A-Tailing Mix were added to end repair. The cDNA fragments were amplified by PCR and products were purified using Ampure XP Beads. The double-strand PCR products were denatured and circularised by the splint oligo sequence to construct the final library. Then the single-strand circle DNA was formatted as the final library. The final library was amplified by phi29 to produce a DNA nanoball (DNB) with more than 300 copies of one molecule. DNBs were loaded into patterned nanoarray and single end 50 bases reads were generated on the BGISEQ500 platform (BGI, Shenzhen, China). HISAT2 (v2.0.4) was used to map the clean reads to the genome. Bowtie2 (v2.2.5) was applied to align the clean reads to the reference coding gene set. RSEM (v1.2.12) was used to calculate the expression level of the gene. Differentially expressed genes (DEGs) with a fold change > 0 and P -value < 0.05 were determined using DESeq2 (v1.4.5).

Transmission electron microscopy

Mice LV tissues were fixed with 2.5% glutaraldehyde overnight at 4°C. After washing three times with cacodylate buffer, post-fixation with 1% osmium tetroxide was performed for 2 h at

room temperature. Following washing three times with phosphate buffer, samples were dehydrated with a series of graded ethanol. Then samples were embedded and polymerised. Ultrathin sections to 60 nm were prepared and stained with lead citrate and uranyl acetate. The sections were imaged with a transmission electron microscope (HITACHI, Tokyo Japan). Intermyofibrillar mitochondrial morphology was analysed by ImageJ. After manually tracing mitochondria on electron micrographs, mitochondrial area, perimeter, form factor $[(\text{perimeter}^2)/(4\pi \times \text{area})]$ and circularity $[(4\pi \times \text{area})/(\text{perimeter}^2)]$ were analysed as to their shape descriptor. At least 330 mitochondria per sample were scored and the quantification was performed blinded to conditions.

Mitochondrial respiration assessment

Cellular oxygen consumption rate (OCR) was analysed using the Seahorse extracellular flux (XF) 96 analyser (Agilent, Lexington, USA). A total of 8000 cardiac myocytes were seeded on a Seahorse microplate in 80 μL growth medium overnight. On the day of the Seahorse assay, cells were switched to Seahorse XF base medium with supplements as described below and maintained in a CO₂-free incubator at 37°C for 1 h. For the mitochondrial stress test, the XF base medium was supplemented with 10 mM glucose, 1 mM pyruvate and 2 mM glutamine. OCR was continuously monitored at each of the following phases: baseline and following sequential addition of oligomycin (1.5 μM), carbonyl cyanide-ptrifluoromethoxyphenyl-hydrazone (2 μM) and a mixture of rotenone/antimycin A (0.5 μM). Data were acquired and analysed using Wave software (Agilent, California, USA).

Statistics

Continuous data were evaluated by the Student's t -test or the Mann-Whitney U -test. Categorical data were compared by the χ^2 test or Fisher's exact test, as appropriate. A two-tailed P -value < 0.05 was considered statistically significant. Statistical analysis was performed using the IBM SPSS Statistics 26.0 software.

ACKNOWLEDGMENTS

This work was supported by the Natural Science Foundation of Shanghai (23ZR1420700) and the Shanghai 'Rising Stars of Medical Talents' Youth Development Program – Youth Medical Talents – Specialist Program.

AUTHOR CONTRIBUTIONS

Hao Zhang: Conceptualization; data curation; formal analysis; funding acquisition; investigation; methodology; project administration; resources; software; supervision; validation; visualization; writing – original draft; writing – review and editing. **Yunjing Shi:** Conceptualization; data curation; formal analysis; funding acquisition; investigation; methodology; project administration; resources; software; supervision; validation; visualization; writing – original draft; writing – review and editing. **Yingze Fan:** Investigation; methodology; software; validation. **Dehao**

Zhu: Data curation; formal analysis; methodology; software. **Zeping Qiu:** Conceptualization; project administration; resources; validation; visualization. **Huihui Chi:** Investigation. **Qiongyi Hu:** Conceptualization; supervision; visualization. **Liangzhe Xie:** Data curation; investigation; methodology; validation. **Yue Sun:** Conceptualization; investigation; methodology; resources. **Honglei Liu:** Investigation. **Xiaobing Cheng:** Investigation. **Junna Ye:** Investigation. **Hui Shi:** Investigation. **Zhuochao Zhou:** Conceptualization; investigation; methodology. **Jianfen Meng:** Investigation. **Jialin Teng:** Investigation. **Chengde Yang:** Investigation. **Wei Jin:** Conceptualization; funding acquisition; project administration; resources; validation; visualization; writing – review and editing. **Yutong Su:** Funding acquisition; writing – review and editing.

CONFLICT OF INTEREST

The authors declare no conflict of interest.

ETHICS APPROVAL AND CONSENT TO PARTICIPATE

The study was performed in accordance with the Declaration of Helsinki and the Principles of Good Clinical Practice. Biological samples were obtained under a protocol approved by the Institutional Research Ethics Committee of Ruijin Hospital (ID: 2016-62), Shanghai, China. All subjects gave written informed consent. All animal experiments were performed in accordance with the Guide for the Care and Use of Laboratory Animals, approved by the Animal Care and Use Committee of Shanghai Jiao Tong University School of Medicine (China) and followed the US National Institutes of Health Using Animals in Intramural Research guidelines for animal use.

REFERENCES

- Reeves WH, Nigam SK, Blobel G. Human autoantibodies reactive with the signal-recognition particle. *Proc Natl Acad Sci USA* 1986; **83**: 9507–9511.
- Suzuki S, Nishikawa A, Kuwana M et al. Inflammatory myopathy with anti-signal recognition particle antibodies: Case series of 100 patients. *Orphanet J Rare Dis* 2015; **10**: 61.
- Watanabe Y, Uruha A, Suzuki S et al. Clinical features and prognosis in anti-SRP and anti-HMGR necrotizing myopathy. *J Neurol Neurosurg Psychiatry* 2016; **87**: 1038–1044.
- Gupta R, Wayangankar SA, Targoff IN, Hennebry TA. Clinical cardiac involvement in idiopathic inflammatory myopathies: A systematic review. *Int J Cardiol* 2011; **148**: 261–270.
- Lilleker JB, Roberts M, Diederichsen L. Cardiac involvement in inflammatory myopathies and inherited muscle diseases. *Curr Opin Rheumatol* 2020; **32**: 528–533.
- Betteridge Z, Tansley S, Shaddick G et al. Frequency, mutual exclusivity and clinical associations of myositis autoantibodies in a combined European cohort of idiopathic inflammatory myopathy patients. *J Autoimmun* 2019; **101**: 48–55.
- Dankó K, Ponyi A, Constantin T, Borgulya G, Szegedi G. Long-term survival of patients with idiopathic inflammatory myopathies according to clinical features: A longitudinal study of 162 cases. *Medicine (Baltimore)* 2004; **83**: 35–42.
- Fairley JL, Wicks I, Peters S, Day J. Defining cardiac involvement in idiopathic inflammatory myopathies: A systematic review. *Rheumatology (Oxford)* 2021; **61**: 103–120.
- Shi Y, Zhang H, Qiu Z et al. Value of the HFA-PEFF diagnostic algorithms for heart failure with preserved ejection fraction to the inflammatory myopathy population. *Arthritis Res Ther* 2023; **25**: 141.
- Lee JH, Chandrasekar S, Chung S et al. Sequential activation of human signal recognition particle by the ribosome and signal sequence drives efficient protein targeting. *Proc Natl Acad Sci USA* 2018; **115**: e5487–e5496.
- Benveniste O, Drouot L, Jouen F et al. Correlation of anti-signal recognition particle autoantibody levels with creatine kinase activity in patients with necrotizing myopathy. *Arthritis Rheum* 2011; **63**: 1961–1971.
- Valiyil R, Casciola-Rosen L, Hong G, Mammen A, Christopher-Stine L. Rituximab therapy for myopathy associated with anti-signal recognition particle antibodies: A case series. *Arthritis Care Res (Hoboken)* 2010; **62**: 1328–1334.
- Zhang H, Sun Y, Liu H et al. Plasma exchange therapy in refractory inflammatory myopathy with anti-signal recognition particle antibody: A case series. *Rheumatology (Oxford)* 2022; **61**: 2625–2630.
- Rojana-udomsart A, Mitrapant C, Bundell C et al. Complement-mediated muscle cell lysis: A possible mechanism of myonecrosis in anti-SRP associated necrotizing myopathy (ASANM). *J Neuroimmunol* 2013; **264**: 65–70.
- Bergua C, Chiavelli H, Allenbach Y et al. In vivo pathogenicity of IgG from patients with anti-SRP or anti-HMGR autoantibodies in immune-mediated necrotizing myopathy. *Ann Rheum Dis* 2019; **78**: 131–139.
- Ladislau L, Arouche-Delaperche L, Allenbach Y, Benveniste O. Potential pathogenic role of anti-signal recognition protein and Anti-3-hydroxy-3-methylglutaryl-CoA reductase antibodies in immune-mediated necrotizing myopathies. *Curr Rheumatol Rep* 2018; **20**: 56.
- Wang L, Liu L, Hao H et al. Myopathy with anti-signal recognition particle antibodies: Clinical and histopathological features in Chinese patients. *Neuromuscul Disord* 2014; **24**: 335–341.
- Allenbach Y, Benveniste O, Stenzel W, Boyer O. Immune-mediated necrotizing myopathy: Clinical features and pathogenesis. *Nat Rev Rheumatol* 2020; **16**: 689–701.
- Takeguchi-Kikuchi S, Hayasaka T, Katayama T et al. Anti-signal recognition particle antibody-positive necrotizing myopathy with secondary cardiomyopathy: The first myocardial biopsy- and multimodal imaging-proven case. *Intern Med* 2019; **58**: 3189–3194.
- Wang H, Liu HX, Wang YL, Yu XQ, Chen XX, Cai L. Left ventricular diastolic dysfunction in patients with dermatomyositis without clinically evident cardiovascular disease. *J Rheumatol* 2014; **41**: 495–500.

21. Diederichsen LP, Simonsen JA, Diederichsen AC *et al.* Cardiac abnormalities in adult patients with polymyositis or dermatomyositis as assessed by noninvasive modalities. *Arthritis Care Res (Hoboken)* 2016; **68**: 1012–1020.
22. Lu Z, Wei Q, Ning Z, Qian-Zi Z, Xiao-Ming S, Guo-Chun W. Left ventricular diastolic dysfunction – early cardiac impairment in patients with polymyositis/dermatomyositis: A tissue Doppler imaging study. *J Rheumatol* 2013; **40**: 1572–1577.
23. Römisch K, Miller FW, Dobberstein B, High S. Human autoantibodies against the 54 kDa protein of the signal recognition particle block function at multiple stages. *Arthritis Res Ther* 2006; **8**: R39.
24. Okazaki Y, Ohno H, Takase K, Ochiai T, Saito T. Cell surface expression of calnexin, a molecular chaperone in the endoplasmic reticulum. *J Biol Chem* 2000; **275**: 35751–35758.
25. Yanase K, Madaio MP. Nuclear localizing anti-DNA antibodies enter cells via caveoli and modulate expression of caveolin and p53. *J Autoimmun* 2005; **24**: 145–151.
26. Yanase K, Smith RM, Puccetti A, Jarett L, Madaio MP. Receptor-mediated cellular entry of nuclear localizing anti-DNA antibodies via myosin 1. *J Clin Invest* 1997; **100**: 25–31.
27. Li Y, Heuser JS, Cunningham LC, Kosanke SD, Cunningham MW. Mimicry and antibody-mediated cell signaling in autoimmune myocarditis. *J Immunol* 2006; **177**: 8234–8240.
28. Luptak I, Sverdlov AL, Panagia M *et al.* Decreased ATP production and myocardial contractile reserve in metabolic heart disease. *J Mol Cell Cardiol* 2018; **116**: 106–114.
29. Kumar AA, Kelly DP, Chirinos JA. Mitochondrial dysfunction in heart failure with preserved ejection fraction. *Circulation* 2019; **139**: 1435–1450.
30. Ráduly AP, Sárkány F, Kovács MB *et al.* The novel cardiac myosin activator danicamtiv improves cardiac systolic function at the expense of diastolic dysfunction in vitro and in vivo: Implications for clinical applications. *Int J Mol Sci* 2022; **24**: 446.
31. Miranda-Silva D, G Rodrigues P, Alves E *et al.* Mitochondrial reversible changes determine diastolic function adaptations during myocardial (reverse) remodeling. *Circ Heart Fail* 2020; **13**: e006170.
32. Tong D, Schiattarella GG, Jiang N *et al.* NAD⁺ repletion reverses heart failure with preserved ejection fraction. *Circ Res* 2021; **128**: 1629–1641.
33. Meyer A, Laverny G, Allenbach Y *et al.* IFN- β -induced reactive oxygen species and mitochondrial damage contribute to muscle impairment and inflammation maintenance in dermatomyositis. *Acta Neuropathol* 2017; **134**: 655–666.
34. Zhong D, Wu C, Bai J, Xu D, Zeng X, Wang Q. Co-expression network analysis reveals the pivotal role of mitochondrial dysfunction and interferon signature in juvenile dermatomyositis. *PeerJ* 2020; **8**: e8611.
35. Bohan A, Peter JB. Polymyositis and dermatomyositis (first of two parts). *N Engl J Med* 1975; **292**: 344–347.
36. Hoogendijk JE, Amato AA, Lecky BR *et al.* 119th ENMC international workshop: Trial design in adult idiopathic inflammatory myopathies, with the exception of inclusion body myositis, 10–12 October 2003, Naarden, The Netherlands. *Neuromuscul Disord* 2004; **14**: 337–345.

Supporting Information

Additional supporting information may be found online in the Supporting Information section at the end of the article.



This is an open access article under the terms of the [Creative Commons Attribution-NonCommercial-NoDerivs](#) License, which permits use and distribution in any medium, provided the original work is properly cited, the use is non-commercial and no modifications or adaptations are made.